Available online at www.sciencedirect.com
SCIENCE DIRECT
Journal of Catalysis 232 (2005) 199–209
JOURNAL OF CATALYSIS
www.elsevier.com/locate/jcat

Carbon-supported Pt–Sn electrocatalysts for the anodic oxidation of H_2, CO, and H_2/CO mixtures. Part I. Microstructural characterization

V. Radmilovic [a], T.J. Richardson [b], S.J. Chen [a], P.N. Ross Jr. [b,*]

[a] *National Center for Electron Microscopy (NCEM), Ernest Orlando Lawrence Berkeley National Laboratory, Berkeley, CA 94720, USA*
[b] *Materials Sciences Division, Ernest Orlando Lawrence Berkeley National Laboratory, Berkeley, CA 94720, USA*

Received 29 November 2004; revised 1 March 2005; accepted 4 March 2005

Available online 12 April 2005

Abstract

High-resolution transmission electron microscopy (HRTEM), microchemical analysis by X-ray emission spectroscopy (EDS), and X-ray diffraction (XRD) were used to characterize the composition, size, distribution, and morphology of the phases present in three different carbon-supported Pt–Sn catalysts. The catalysts had nominal Pt/Sn atomic ratios of 1:1 (500N and 900N samples) and 3:1 (E270 sample). The 1:1 catalyst sample heat-treated at 500 °C (500N) contained a Pt-rich fcc alloy phase ($a_0 = 0.3965$ nm) and tetragonal SnO_2. The sample from the same precursors heat treated at 900 °C (900N) consisted of stoichiometric hexagonal PtSn, a nearly stoichiometric Pt_3Sn fcc phase ($a_0 = 0.3988$ nm), and tetragonal SnO_2. Neither pure tin nor pure platinum particles were detected in any of the catalysts. The 3:1 catalyst sample reduced in H_2 at 270 °C (E270) was composed entirely of the stoichiometric Pt_3Sn cubic phase ($a_0 = 0.3998$ nm). The Pt_3Sn-type particles are predominantly single nanocrystals with mean diameters of ∼4 nm (for the catalysts E270 and 500N) and ∼5 nm (for the catalyst 900N), whereas the PtSn particles were larger. The Pt_3Sn-type particles in 500N and 900N were generally highly faceted, with {111} and {200} facets, whereas the E270 catalyst had generally a smooth spheroidal outline. Whereas the Pt_3Sn particles in the E270 and 900N catalysts were equiaxed, in the 500N catalyst the alloy particles had uniquely elongated (e.g., ellipsoidal) shapes.

Keywords: Platinum; Platinum–tin; Electrocatalysts; Electron microscopy; Electron diffraction; X-Ray diffraction

1. Introduction

The microstructure of bimetallic Pt–Sn catalysts with oxide supports, such as alumina and silica, are of particular interest for a variety of applications in heterogeneous catalysis [1–8]. Although the reasons for the superior properties of these catalysts in hydrocarbon refining are not fully understood, the dispersion, structure, and compositional homogeneity of the alloy clusters are all clearly important factors in determining their catalytic activity. Various characterization techniques, mainly X-ray diffraction [1–3,7,8] and transmission electron microscopy (TEM) [4–6], have been applied to identify the composition and microstructure of Pt–Sn-based catalysts. However, conflicting conclusions have been reported. Kuznetsov et al. [7] reported that platinum forms practically all possible alloys with tin. However, Srinivasan et al. [1] examined the reduction of a Pt–Sn-chloride precursor on alumina in hydrogen by in situ XRD and observed PtSn (1:1) to be the only alloy phase formed. In a later XRD study from the same laboratory [2], for a series of alumina-supported catalysts containing 1 wt% Pt and increasing amounts of Sn to give Pt/Sn mole ratios from 1:1 to 1:10, they reported that PtSn was the only alloy phase present in all of the samples, and the Sn present in excess of that needed for PtSn was in an "X-ray amorphous" form. In subsequent examinations of the same Pt–Sn–Al_2O_3 catalysts by electron microdiffraction, $PtSn_2$ was observed as a minor phase along with PtSn, and metallic Sn was not detected, and the other Sn-containing phases could not be identified [3,4]. Later on, high-resolution TEM was also used, and Davis and co-workers concluded [6] that the dominant alloy formed

* Corresponding author. Fax: +1 510 486 5330.
E-mail address: pnross@lbl.gov (P.N. Ross).

0021-9517/$ – see front matter
doi:10.1016/j.jcat.2005.03.007

on an alumina support was PtSn, and it is only at extreme compositions that a significant fraction of other alloys was present: at low Sn/Pt ratio, clusters of Pt, Pt_3Sn, and PtSn were present, whereas at high Sn/Pt ratios the dominant phases were PtSn, Pt_2Sn_3, and $PtSn_4$. On the other hand, Schwank and co-workers [8] concluded that alloy formation in Pt–Sn catalysts prepared on oxides does not occur to a significant extent. It is difficult to reconcile these contradictory reports. The main conclusion appears to be that it is essential to carefully characterize any supported Pt–Sn catalyst before analyzing kinetic results obtained with these catalysts.

Pt–Sn alloys are among the most active catalysts known for the electrooxidation of syngas or reformate, that is, a H_2-rich H_2/CO mixture. Previous studies with $Pt_3Sn(hkl)$ single crystal electrodes in acid electrolyte have shown that the electrochemical oxidation of carbon monoxide is a strongly structure-sensitive reaction, for which the (111) surface (25 at% Sn) has the highest activity [9,10]. However, much less work has been done with carbon-supported Pt–Sn catalysts than with oxide-supported Pt–Sn catalysts [11]. The structure sensitivity of this reaction for H_2/CO electrooxidation on Pt_3Sn means that the activity of the supported catalysts will probably depend on more than just the particle size of the Pt_3Sn alloy phase. In addition, there are reports of a promotional effect for H_2/CO electrooxidation of carbon-supported Pt impregnated with non-alloyed SnO_x phase(s) [12,13]. Thus, one should expect very preparation-sensitive activity for carbon-supported Pt–Sn catalysts in this reaction, and to understand this sensitivity it is essential to have detailed characterizations of all phases present.

In the present work, we examine three different carbon-supported bimetallic Pt–Sn catalysts by high-resolution transmission electron microscopy (HRTEM), electron and X-ray diffraction techniques, and microchemical analysis by energy-dispersive X-ray spectroscopy (EDS), following procedures previously used in this laboratory for the characterization of carbon-supported Pt–Ru catalysts [14]. The size of the particles presents challenges to microstructural characterization. Many of these problems can be addressed by transmission electron microscopy, particularly by high-resolution electron microscopy, which reveals the presence of defects such as dislocations, twins, etc. The advantages of the TEM in catalyst characterization have been described in several recently published review articles [15–17]. HREM has been extensively used to determine faceting planes, geometric shapes, the presence of surface steps, surface roughness, and size distribution of the Pt–Sn particles. Weak-beam dark-field imaging (WBDF) was not used here because of its well-known limitations for particle sizes below 10 nm [17–20]. The catalytic activity and the relationship of activity to microstructure of the catalysts analyzed here are presented in Part II.

2. Experimental

2.1. Catalyst preparation

The Pt–Sn catalysts studied here (samples 500N and 900N) were supplied by the Johnson Matthey Technology Center (Reading, UK), and the third one (denoted E270) was supplied by E-Tek (Somerset, NJ, USA). An acetylene black (Shawinigan) carbon support with a Pt/Sn stoichiometry of 1.23:1 and a metal loading of 23 wt% was used for the 500N and 900N samples. They were made by a conventional precipitation route [13], but differed in the thermal treatment they received to decompose the precursor (500 or 900 °C, respectively, in an atmosphere of N_2) and promote alloying of the two metals. For the E-Tek sample, prepared by a proprietary method, Vulcan XC-72 (Cabot) carbon black, a stoichiometry of 3:1, and a metal loading of 20 wt% were used; the final step in preparation reduction in H_2 was carried out at 270 °C.

2.2. Electron microscopy

We prepared specimens for transmission electron microscopy by making suspensions of the catalyst powders in ethanol, in an ultrasonic bath. These suspensions were dropped onto clean holey carbon grids, which were then dried in air. Samples were examined with the OO2B, the ARM high-resolution electron microscopes, and the JEOL 200CX analytical electron microscope at NCEM [21]. Particle size distributions were determined from images of, on average, 20 different regions of the catalyst; each region contained 10–20 particles. The particle shapes were determined by real space crystallography with the use of high-resolution images taken from particles near or on the edge of the carbon black substrate, and/or by numerical Fourier filtering of the digitized image intensity spectrum of particles on top of the carbon black. Dark-field imaging was also used to investigate the overall distribution of Pt–Sn particles. To avoid contamination during energy-dispersive X-ray spectroscopy (EDS) analysis, microchemical analysis was performed at −160 °C, with a cold stage with a beryllium holder. This was found to be essential, because the time required to collect statistically reliable spectra from 2-nm particles (or particle clusters) with the use of a 10-nm electron beam is very long. The fluorescence effect from such a small probe beam can be neglected [22].

2.3. X-ray diffraction

XRD patterns for the catalyst powder samples were acquired with a Siemens D5000 diffractometer, operating in Bragg–Brentano mode. Cu K_β radiation was eliminated with a diffracted-beam graphite monochromator. Because of the relatively low metal loading on the low-density carbon support, data collection periods of up to 10 h were required. The

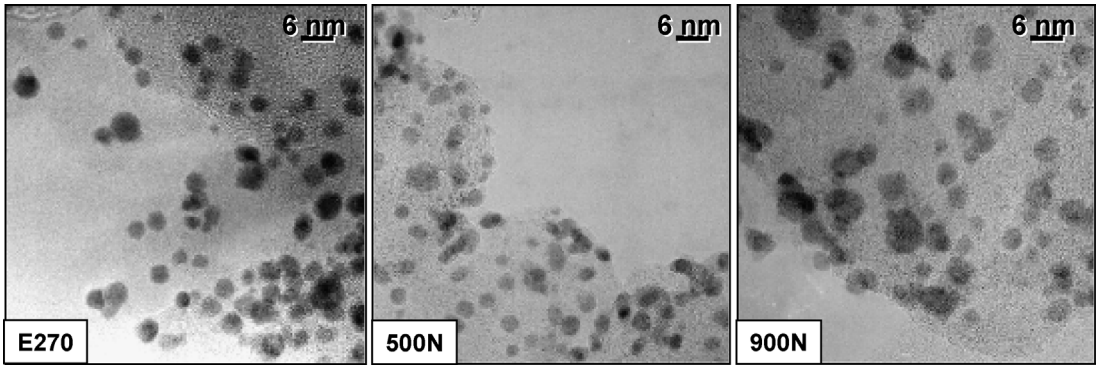

Fig. 1. Low magnification HREM micrographs of Pt–Sn catalysts supported on carbon black: E270, 500N, and 900N.

patterns were analyzed by Rietveld refinement, with the program RIQAS (Materials Data, Inc., Livermore, CA). Both $K_{\alpha 1}$ and $K_{\alpha 2}$ reflections were included in the refinements.

3. Results and discussion

3.1. Transmission electron microscopy

Low-magnification transmission electron micrographs of Pt–Sn catalysts supported on carbon black are shown in Fig. 1. At this magnification, there is little apparent difference between these catalysts; all of them have particles uniformly dispersed over the carbon particle surfaces with sizes nominally in the same range (6 ± 3 nm) and the same general shape (spheroidal). The presence of particles with distinctly different phases/compositions, such as SnO_2 versus Pt, is not obvious in these micrographs. At higher resolution, however, differences in particle shape and composition become readily apparent.

Two-dimensional projections in high-resolution images, such as those for E270 in Fig. 2a, give the impression of spherical or elliptical shapes, as opposed to faceted shapes, such as cubo-octahedral-octahedral, as we had observed for Pt–Ru catalysts [14,23]. Apparent rounding of particles can be caused by two effects. Because of inclination of the particles from the low index zone axis, faceted corners appear to be slightly curved [24]; even when particles are aligned along a low index zone axis they can appear to be spherical because of interference from the carbon substrate and confusing contrast that obscures sharp edges and corners [25]. The latter effect can be avoided by an analysis of particles in the thinner regions of the substrate, for example, close to the edge of the carbon support, such as those shown in Fig. 2b. Because the majority of the particles in the catalysts are not conveniently located on edges of the carbon substrate, however, analysis of only these particles may not be representative of the catalyst as a whole. In the same catalyst (E270), when the particles are far from the edge of carbon black support, even when the particles are aligned on the zone axis, the particle edges still appear rounded (Fig. 3a). The contrast problem with particles on the thick regions of the

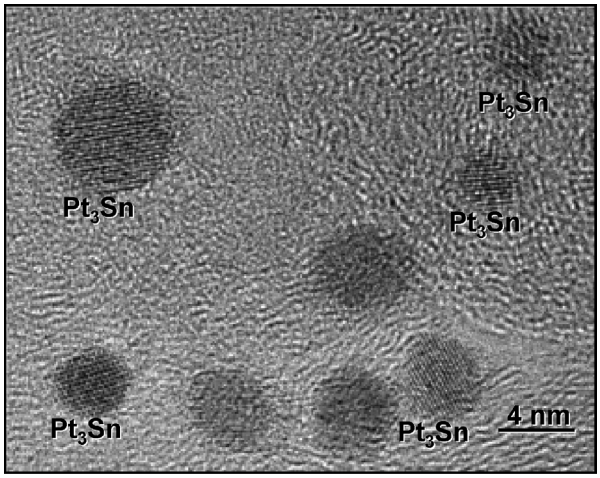

(a)

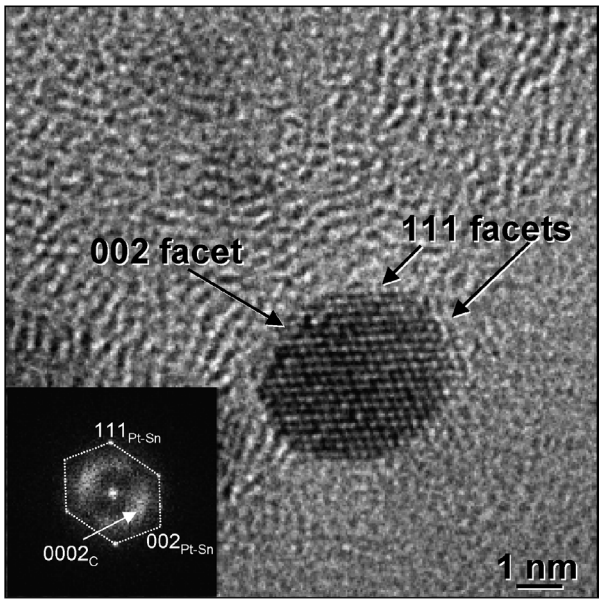

(b)

Fig. 2. HREM micrographs of Pt_3Sn particles in catalyst E270 with different apparent shapes: (a) apparent rounding of particles due to interference from carbon; (b) faceted particles observed on the edges of the carbon support.

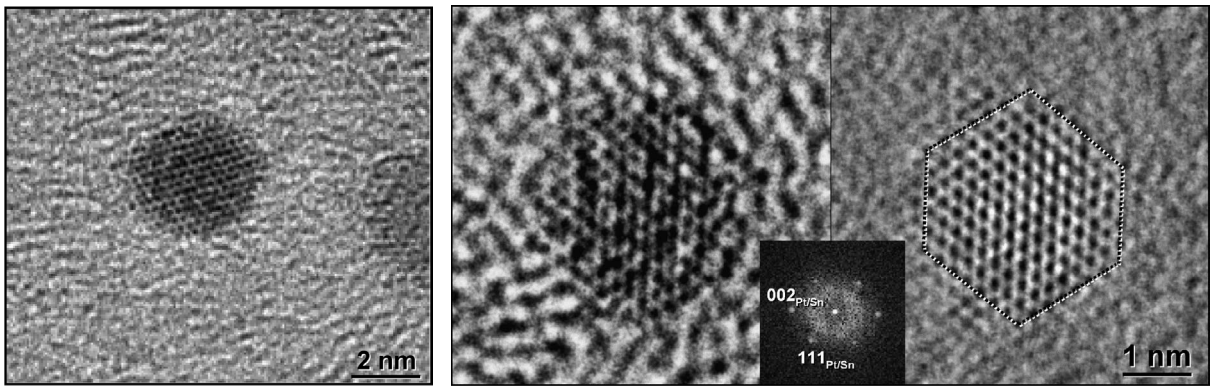

(a) (b)

Fig. 3. HREM micrographs of a single Pt_3Sn particle in catalyst E270: (a) aligned on the 110 zone axis; (b) Fourier filtering of carbon scattering reveals faceted shapes.

Table 1
Crystallographic data for Pt and Sn phases [37]

Formula	Lattice parameters (nm)			Structure type	Space group
	a	*b*	*c*		
a-Sn	0.64892			Diamond	*Fd*3*m* (227)
β-Sn	0.58313		0.31815	β-Sn	$I4_1/amd$ (141)
SnO_2	0.4738		0.3187	TiO_2 (Rutile)	*P*42/*mnm* (136)
Pt	0.39242			Cu	*Fm*3*m* (225)
Pt_3Sn	0.40005			Cu_3Au	*Pm*3*m* (221)
Pt_2Sn_3	0.43345		1.29606	Pt_2Sn_3	$P6_3/mmc$ (194)
PtSn	0.4104		0.5436	AsNi	$P6_3/mmc$ (194)
$PtSn_2$	0.64331			CaF_2	*Fm*3*m* (225)
$PtSn_4$	0.63823	0.64190	1.13666	$PdSn_4$	*Aba*2 (41)

Table 2
Plane spacings for possible pairs of metals and/or alloys

Phase 1	{*hkl*} *d* (nm)	Phase 2	{*hkl*} *d* (nm)	Difference (%)
Pt	{111} 0.2265	$PtSn_2$	{220} 0.2274	0.42
Pt_2Sn_3	{004} 0.3234	$PtSn_4$	{020} 0.3209	0.74
$PtSn_2$	{002} 0.3217	Pt_2Sn_3	{004} 0.3234	0.53
Pt_3Sn	{111} 0.2309	a-Sn	{220} 0.2294	0.67
$PtSn_4$	{131} 0.1997	Pt_3Sn	{200} 0.2000	0.14
Pt_2Sn_3	{110} 0.2163	PtSn	{102} 0.2159	0.16

carbon was reduced by Fourier filtering, which can remove much of the contribution from the incoherent scattering of electrons from the amorphous carbon. As shown in Fig. 3b, Fourier filtered images from particles in the interior of catalyst also reveal faceted shapes, typically cubo-octahedral. All in all, we concluded that particles in E270 are highly crystalline and faceted. As we show below, further analysis of lattice spacing in both individual particles (lattice imaging and selected area diffraction) and overall (X-ray diffraction) indicates that essentially all particles in this catalyst are in the Pt_3Sn alloy phase.

High-resolution images of the 500N and 900N samples reveal significantly different microstructures from the E270 catalyst. Lattice imaging at high resolution, in principle, can be used to identify the crystallographic phase of individual particles. A summary of the crystal structure structures of the most probable phases present in these catalysts is given in Table 1, and the relevant *d*-spacing for high-symmetry planes of the different phases is summarized in Table 2. Taking into account the effects of sample tilt and uncertainty about the exact direction of the surface normal, along with strong Fresnel effects in small particles, Radmilovic et al. [26] have calculated that the errors in the measurement of interplanar spacing in high-resolution images are on the order of a few percent and can be as high as 10%. It was not possible, therefore, to make a distinction between the metallic phases in Table 2 by lattice imaging *alone*, because the artificial effects and the experimental error of spacing measured from high-resolution images exceed by many times the difference in interplanar spacing. However, with the crystal symmetry determination from selected area diffraction (SED), it was often possible to identify the crystal phase of individual particles. In particular, the much larger lattice spacing and the symmetry of the SnO_2 phase versus made it possible to identify particles with this phase, as shown for the 500N and 900N samples in Figs. 4a and 4b, respectively. Of particular interest from a catalytic perspective was the distribution of SnO_2 particles relative to fcc particles (e.g., Pt or Pt_3Sn). The relationship seen in Fig. 4 was representative of the distribution of SnO_2 in both samples. In every case where SnO_2 particles could be clearly identified, they were clustered (i.e., in physical contact) with Pt or Pt_3Sn alloy particles. The selected area diffraction pattern from the same region, shown as an inset in Fig. 4a, shows the presence of an fcc phase with a lattice parameter of 0.39 nm, permitting the identification of some Pt or Pt_3Sn particles, as indicated in Figs. 4a and 4b. The physical contact between SnO_2 and Pt particles would be an essential requirement for a synergistic or "promotional" effect of SnO_2 on the Pt, as some have proposed [12,13]. In the case of the 500N and 900N samples, there is direct evidence that such physical contact does occur, and as far as TEM analysis can reveal, this intimate mixing of Pt (or Pt_3Sn alloy) particles and SnO_2 particles is characteristic of all of the SnO_2 particles present. In the case of the 900N sample, in addition the SED pattern

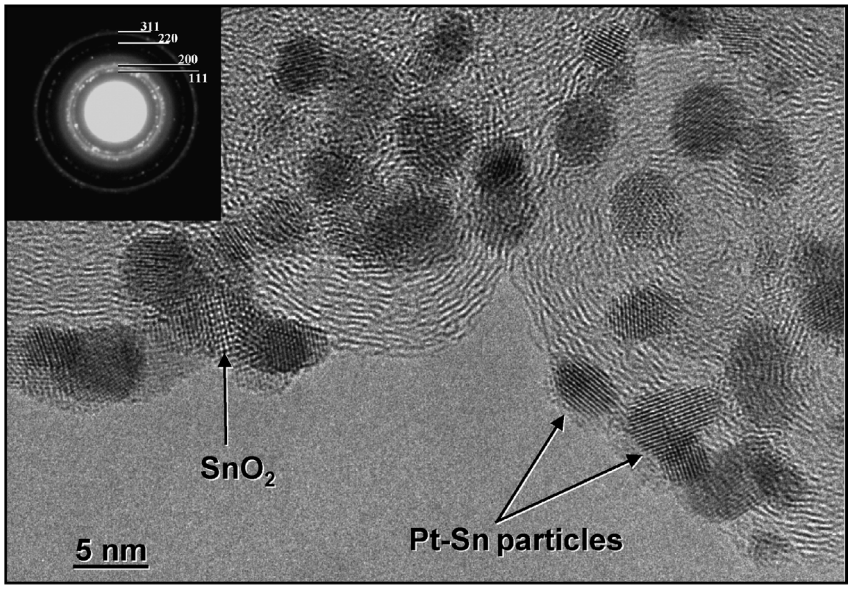

(a)

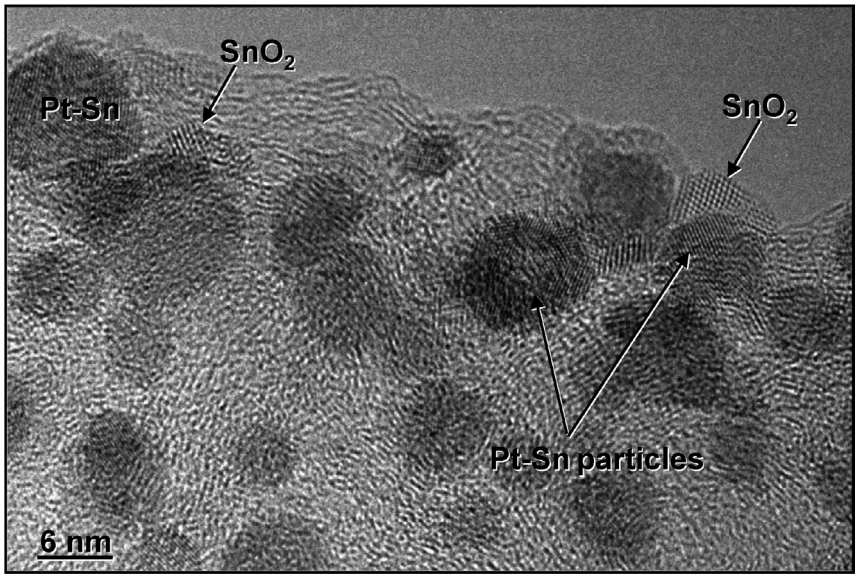

(b)

Fig. 4. HREM micrographs of SnO_2 and Pt–Sn particles in the (a) 500N sample; insert: selected area diffraction (ring) pattern showing an fcc structure with a lattice parameter $a = 0.39$ nm and (b) 900N sample.

from some regions indicated the presence of the hcp alloy PtSn. With proper (and fortuitous) alignment of the fcc and hcp particles, it was possible to distinguish individual PtSn and Pt_3Sn particles in the same field of view with the use of the difference in d-spacing (2.5%) and the lattice fringes, as demonstrated in Fig. 5. PtSn particles were only found in close proximity/contact with Pt_3Sn particles, and never as isolated particles. Presumably this is associated with the preparation chemistry, and the reaction between SnO_2 precursor particles and Pt_3Sn particles necessary to form the PtSn phase.

The three investigated catalysts, E270, 500N, and 900N, have different particle size distributions within the nominal 6 ± 3 nm size regime. Histograms of the particle size distribution are shown in Fig. 6. These histograms include analyses of several different regions in the same catalyst, including some regions where the metal particle distribution was less uniform than that shown in Figs. 1 and 2. The histograms include all particles regardless of phase. The particle size distributions for the E270 and 500N catalysts are quite similar, but the phases are very different. E270 is composed essentially entirely of Pt_3Sn particles, whereas 500N is primarily a mixture of Pt and SnO_2 particles. The 900N catalyst has a classical log-normal distribution function that is characteristic of metallic catalysts that have undergone “sintering” or “coarsening” [27]. In this case, the coarsening in the 900N

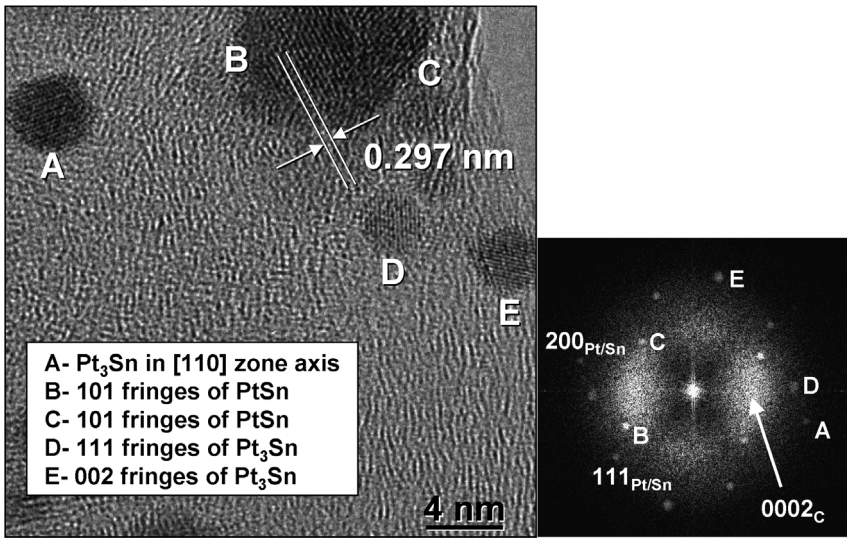

Fig. 5. Identification of PtSn (B and C) and Pt_3Sn (A, D and E) particles in 900N catalyst based on lattice spacing with graphite internal calibration.

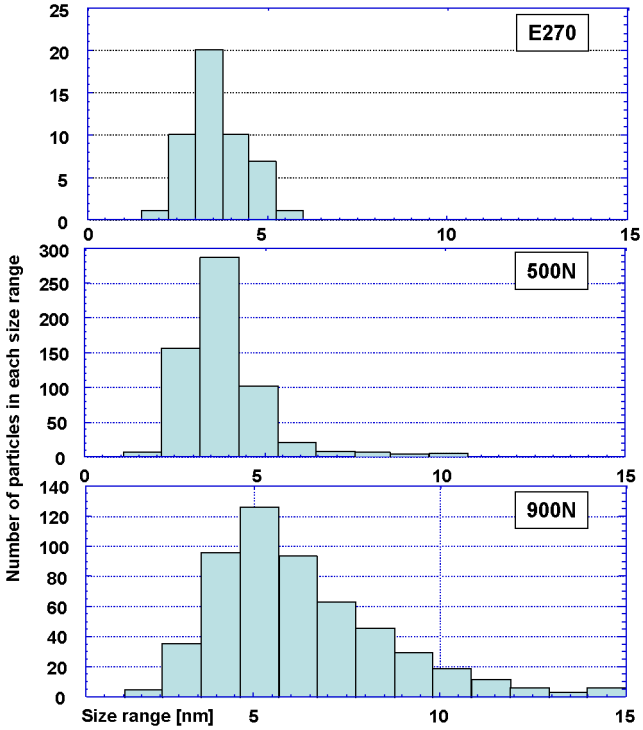

Fig. 6. Histograms of the Pt–Sn particle size distribution in the E270, 500N and 900N catalysts.

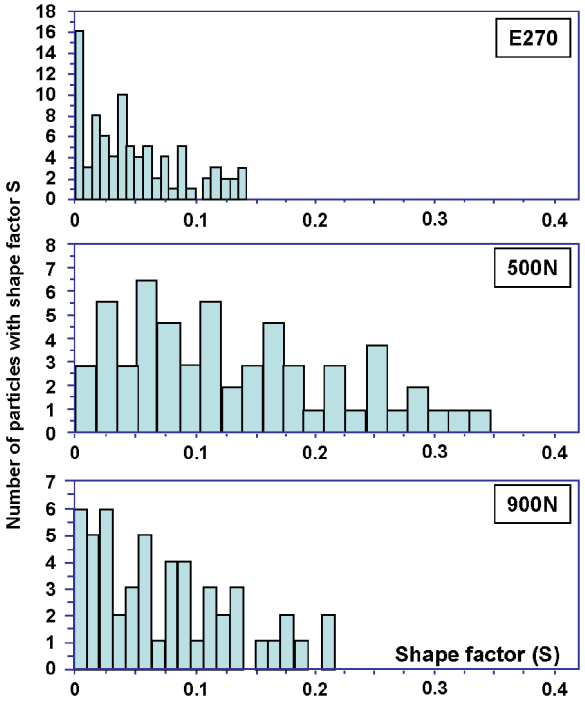

Fig. 7. Histograms of the Pt–Sn particle shapes in E270, 500N and 900N catalysts.

sample is a result of the thermal treatment to promote reaction between the Pt and SnO_2 particles, which apparently also promotes particle growth as well.

The heterogeneous, partially reacted character of the 500N sample could also be seen in the particle shapes. In the E270 sample, which is the most homogeneous sample, most of the particles have an apparently spheroidal shape, which implies that the two-dimensional projection of the three-dimensional shape along the electron beam direction is independent of the particle orientation in the beam. In general, a statistically averaged nonspheroidal shape can be extracted from projected images if the views of a great number of the particles along different directions are available. We used a shape parameter, denoted as S, which is the difference between the longest and shortest dimensions normalized by its size as a numerical measure of the shape of the particle image, such as $S = (d_{\max} - d_{\min})/d_{\text{ave}}$. In the case of an equiaxed particle, S is equal to zero, and the S increases as the particle becomes more stretched to an ellipsoidal or tabular shape. For the E270 sample, most of the S values are concentrated around zero, as shown in Fig. 7.

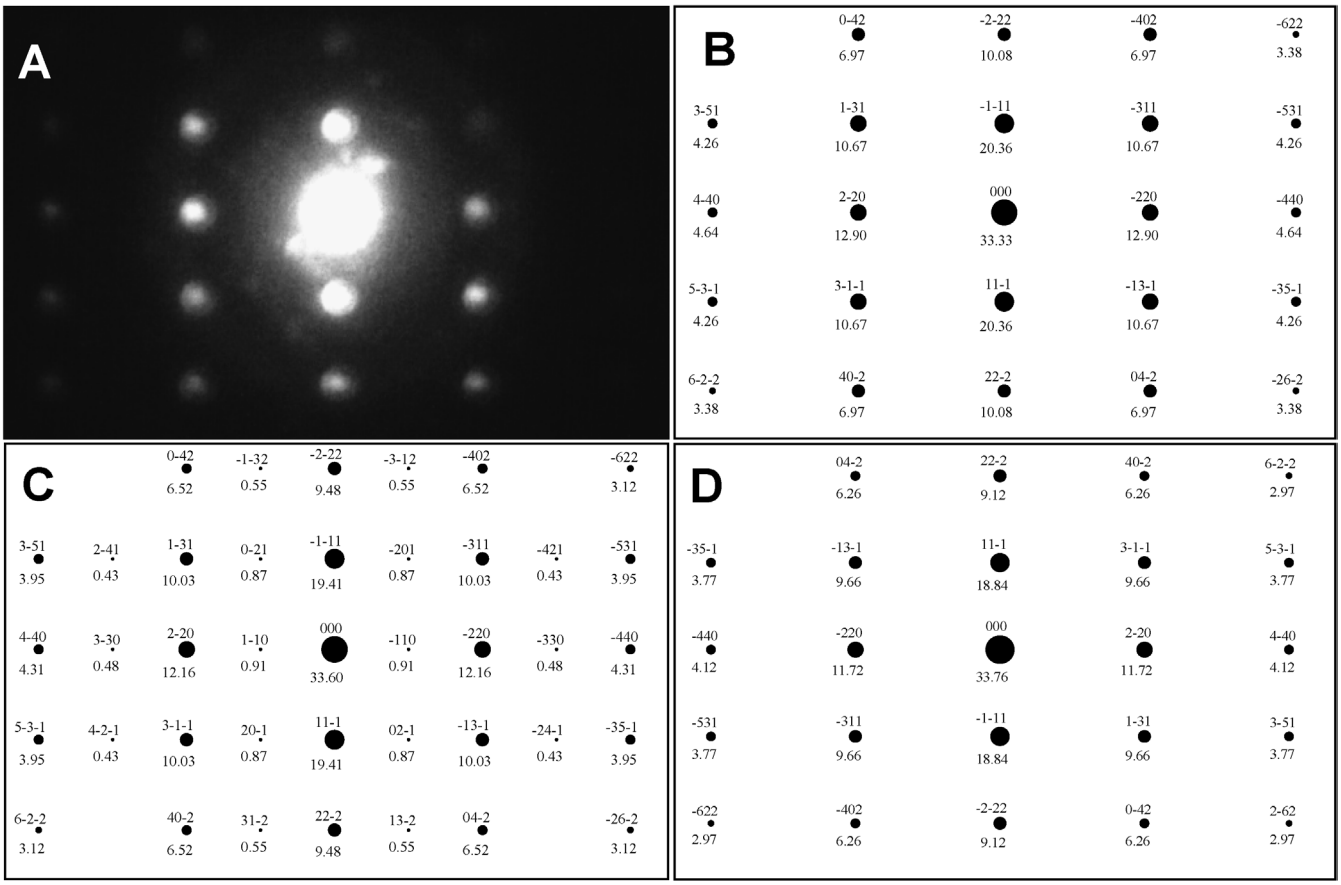

Fig. 8. (A) Nanodiffraction pattern from a single particle in the 900N catalyst and calculated diffraction patterns: (B) fully disordered and (C) fully ordered stoichiometric Pt_3Sn phase; (D) disordered Pt_3Sn phase with non-stoichiometric composition $Pt_{0.7}Sn_{0.3}$. Structure factor value for each reflection is given bellow the diffraction spot.

For 500N, the majority of particles are not equiaxed; the majority *S* factor for Pt–Sn clusters is 0.05–0.15, and some are as high as 0.35, that is, the longest dimension is almost three times longer than the shortest dimension. This is probably a manifestation of both the clustering of Pt and SnO_2 particles and the reaction between Pt and SnO_2 particles to form Pt_3Sn particles with a complex (nonequilibrium) shape. As the reaction between Pt and SnO_2 proceeds to a larger extent at higher temperature in the 900N sample, the resultant Pt_3Sn and PtSn particles are mostly equiaxed, similar to but larger than the Pt_3Sn particles in the E270 catalyst sample.

In some instances, a nanodiffraction pattern could be obtained from a single particle lying on the edge of the carbon substrate. An example of that is shown in Fig. 8A for the 900N sample, indicating an fcc structure in the 112 zone. In comparison, we show the calculated pattern for pure Pt (Fig. 8B), the fully ordered Pt_3Sn phase (Fig. 8C), and a disordered Pt_3Sn phase that is slightly nonstoichiometric (Fig. 8D), with the structure factors for each reflection given below the spot. We never observed the superlattice diffraction spots (Fig. 8C) characteristic of the ordered perfectly stoichiometric compound Pt_3Sn in any of the catalysts, not even in the E270 sample. The calculated DP for a slightly nonstoichiometric Pt_3Sn phase has the best agreement with the experimental NDP in the 900N catalyst. It is possible that the structure factor value for the ordered phase is too small for the superlattice spots to be visible in a DP from a single nanoparticle. As we present below, we did not observe the superlattice reflections in the XRD patterns either, although these reflections are so weak in this Pt–Sn system that they may not be observable above the background from scattering from the carbon (and/or SnO_2 when present).

Occasionally twinned particles were observed with the same {111} twinning plane as in other fcc metals [14], but these occasions were rare, and twinned particles were not considered to be an important characteristic in any of these catalysts. The almost perfect {200} and {111} facets in some of the Pt–Sn bimetallic particles did not appear to be accompanied by any relaxation in the interatomic spacing near the surface, as might occur with a surface enriched in one element relative to the bulk. However, as shown by the data in Table 2, the changes in interplanar spacing in the Pt–Sn system (less than 2.5%) are too small to be observed by lattice imaging of single particles, even when the measurement

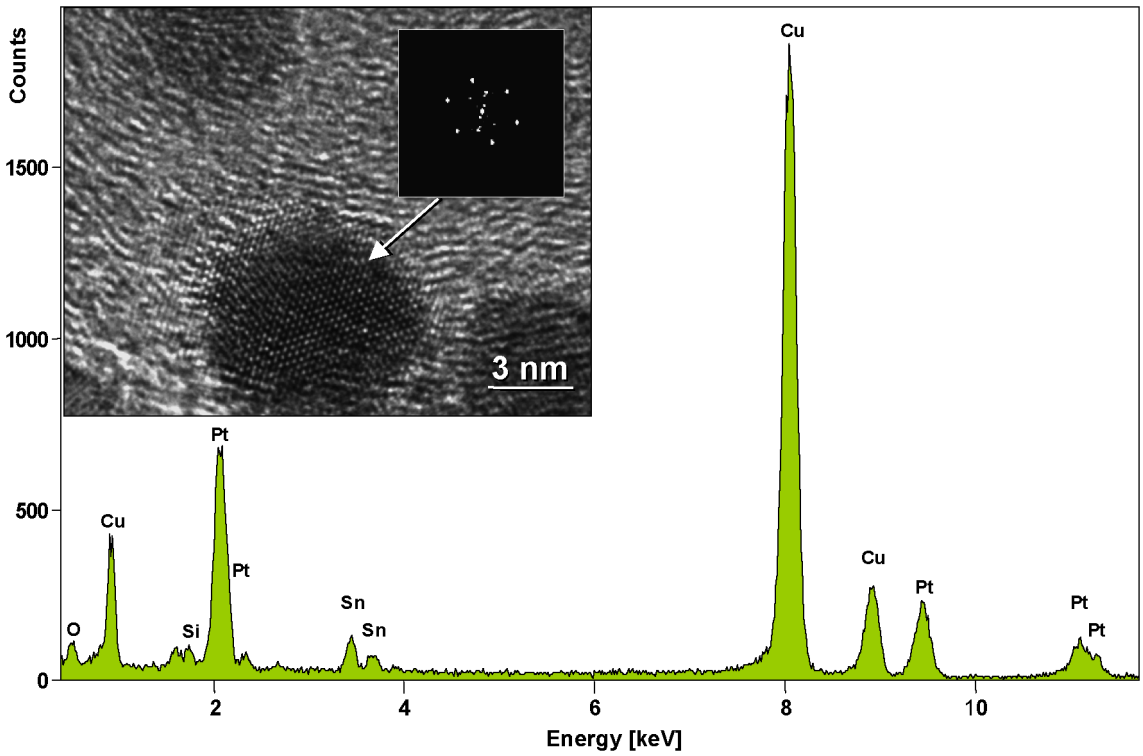

Fig. 9. X-ray fluorescence spectrum taken with sample cooled to −170 °C from the single particle in sample E270 shown in the HREM image (insert) using a 1 nm beam. The Pt/Sn intensity ratio is exactly the same as that in the XRF spectrum from a Pt_3Sn standard.

procedure introduced by Ruijter et al. [28] is applied. The carbon-supported Pt–Sn particles were somewhat unstable under irradiation, and shape changes were seen in some particles on the edge of the carbon support under illumination. Similar behavior has been reported for ultrafine gold particles supported on amorphous Si and SiO_2 [29], MgO [30], or TiO_2 [31] substrates, and in several other pure metals supported on carbon black [31,32], including Pt [33]. Marks and co-workers [30,34] suggested that the reason for this behavior could be a relatively small activation barrier (a few electron volts) for transformations between different shapes compared with the energy deposited by the electron beam. In fact, a large amount of energy is needed to push the particle out of a large potential wall in which the particle is trapped, and once initiated, the particle partially melts, even after the electron-beam intensity is turned down to almost zero [30].

3.2. Microchemical analysis

Elemental analysis from different regions of each sample was conducted with X-ray fluorescence (XRF) spectroscopy with the JEOL 200CX microscope. An ultrathin window detector was used, allowing the presence of oxygen to be detected. A bulk single crystal of Pt_3Sn was used to obtain a calibration factor for the Pt/Sn atomic ratio. XRF analysis of both the 500N and 900N catalysts showed that regardless of the beam size, the Pt/Sn ratio varied over a broad range, but the mean values were 1.50 and 1.36, respectively, which are reasonably close to the ratio in the nominal elemental composition (1.23). This could be explained by the varying amounts of Pt_3Sn and PtSn phases in the analyzed clusters/regions and the presence of clusters with unreacted SnO_2 particles. The latter was more evident in the 500N catalyst, where the relatively high Sn X-ray emission was accompanied by observable oxygen X-ray emission (insignificant in other samples). In the case of the E270 catalyst sample, the Pt/Sn ratio varied much less between different particles, clusters, or regions, but was never as high as the ratio of the nominal composition, that is, from a low of about 1.8 to a high of 2.6, and a mean of 2.3. We have no explanation for why the Pt/Sn ratio from XRF of the E270 sample is lower than the expected value from the bulk composition, 3.0. Typical examples of XRF from the three samples are shown in Fig. 9.

3.3. X-ray diffraction data analysis

The diffraction patterns were analyzed for the presence of known Pt/Sn phases and for Sn and its oxides. The carbon support has only very broad and weak reflections in the 2θ range shown. Its diffraction pattern, therefore, was not refined, but was included in the background calculation. Once approximate quantitative results were obtained, cell parameters and lineshape variables for the individual phases were refined. Observed and calculated patterns for the samples are given in Fig. 10. The E270 sample was essentially entirely of Pt_3Sn; no other phases of either Pt or Sn were observed in this sample. The calculated contributions to the patterns

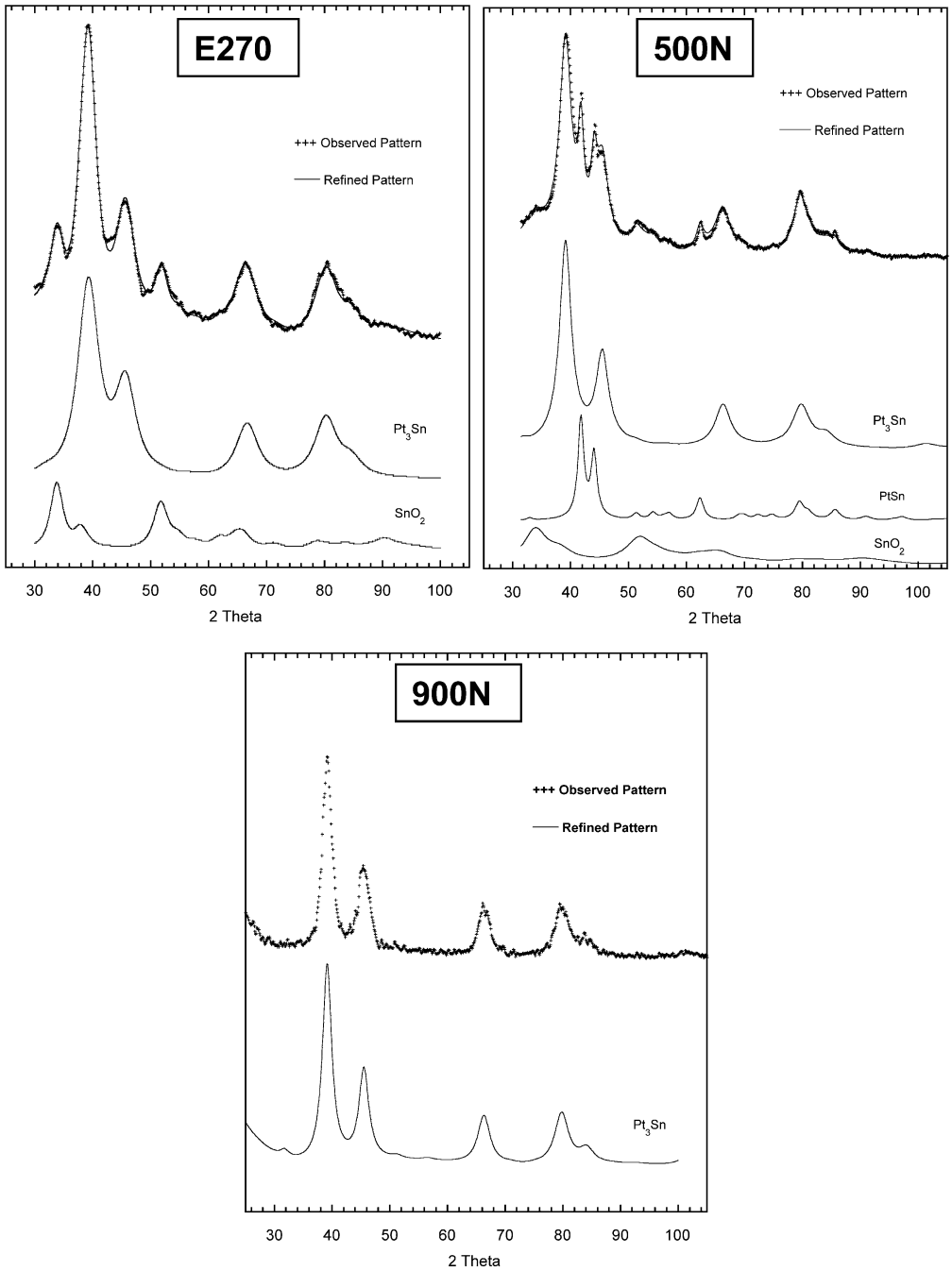

Fig. 10. Quantitative Rietveld refinement of the powder diffraction patterns for the samples: E270, 500N and 900N.

Table 3
Results of XRD refinements and analyses

	mol% Pt_3Sn	mol% PtSn	mol% SnO_2	Pt:Sn atomic ratio	R	R_{wp}
500N	26.4[a]	0	73.6	0.79	0.047	0.055
	$a_0 = 0.3965$ (2)					
	aps[b] = 2.5 nm		aps = 3.5 nm			
900N	13.7	12.1	4.2	0.62	0.048	0.052
	$a_0 = 0.3988$ (5)	$a_0 = 0.4114$ (5)				
		$c_0 = 0.5440$ (6)				
	aps = 3.7 nm	aps = 7.2 nm	aps = 2.1 nm			

[a] Probably two alloys phases, a saturated solid solution and stoichiometric Pt_3Sn (see text).
[b] Average particle size, from refined line shape parameters.

from each phase present in the 500N and 900N samples are summarized in Table 3. In both cases, the XRD analyses reflect considerably lower Pt/Sn atomic ratios than the elemental composition (1.23).

Sample 500N consisted of a Pt–Sn alloy and SnO_2. The refined lattice constant of the alloy was 0.3965 nm, between those of Pt_3Sn (0.4000 nm) and Pt (0.3924 nm). Hansen [35] reports that the solid solubility of Sn in Pt is unknown (as of 1958), but suggests it may be ca. 8 at%. Harris et al. [36] reported a linear dependence of lattice constants for solid solutions of Sn in Pt up to 10% Sn, with a lattice constant of 0.3934 nm for $Pt_{90}Sn_{10}$. They found no evidence for nonstoichiometry in Pt_3Sn and suggested that alloys with 10–25 at% Sn cooled from a melt (at 1365 °C) would separate into two phases, the saturated $Pt_{90}Sn_{10}$ solid solution and stoichiometric Pt_3Sn. Given the near-coincidence of the $Pt_{90}Sn_{10}$ and Pt_3Sn reflections and the particle size broadening, a mixture of $Pt_{90}Sn_{10}$ and stoichiometric Pt_3Sn would produce a diffraction pattern very similar to the refined pattern with a nonstoichiometric Pt_3Sn phase. We conclude that reaction of the Pt and SnO_x precursors at 500 °C most probably results in two alloy phases, $Pt_{90}Sn_{10}$ and Pt_3Sn, in which the average particle size is quite small (Table 3).

The catalyst sample heated to 900 °C reacted more completely. It consisted of a mixture of near-stoichiometric Pt_3Sn ($a_0 = 0.3988$ nm) and stoichiometric PtSn, along with the unreacted SnO_2. The Pt–Sn particles were considerably larger than those in the 500 °C sample, but the average SnO_2 particle size was smaller. The PtSn particles were on average nearly twice the size of the Pt_3Sn particles. This would suggest, as does all of the microscopy, that the alloy phases form by progressive reaction between Pt and Pt_3Sn with SnO_2,

$$0.9Pt + 0.1SnO_2 \rightarrow Pt_{90}Sn_{10} + 0.1O_2,$$
$$Pt_{90}Sn_{10} + 0.15SnO_2 \rightarrow Pt_{75}Sn_{25} + 0.15O_2,$$
$$Pt_{75}Sn_{25} + 0.25SnO_2 \rightarrow Pt_{50}Sn_{50} + 0.25O_2.$$

Although the entire sample was used for XRD data collection, there is considerable discrepancy between the Pt/Sn ratio determined from these refinements and the elemental composition or those determined by the XRF microchemical analysis. Although this may have been due to the considerable overlap of the patterns and the broad contribution from SnO_2, the presence in the 500N and 900N samples of an additional pure Pt or Pt-rich phase with a particle size too small for Rietveld refinement cannot be ruled out.

4. Conclusions

Based on our analysis of carbon-supported Pt–Sn electrocatalysts by high-resolution electron microscopy, microchemical analysis by XRF, and powder X-ray diffraction, we draw the following conclusions:

(1) The three catalysts have significantly different Pt–Sn coordinations and thus should have significantly different catalytic properties if this coordination is important.

(2) The Pt and SnO_2 precursors in the 500N catalyst have only partially reacted to form a relatively small amount of Pt–Sn alloy of uncertain composition. All of the SnO_2 particles appear to be closely associated with Pt particles, such that a catalytically synergistic interaction is plausible (if a synergistic effect exists). The Pt-phase particles are the smallest of the three catalysts, with an average size of ∼3–4 nm.

(3) The higher temperature treatment applied to the 900N catalyst results in more complete reaction between the Pt and SnO_2 precursors, resulting in stoichiometric Pt–Sn alloy particles, Pt_3Sn and PtSn, in roughly equal proportions. The Pt_3Sn particles are slightly larger than the Pt-phase particles in the 500N catalyst, but the PtSn particle size is significantly larger, with an average size of ∼7 nm.

(4) The E270 catalyst, prepared with completely different chemistry, is composed entirely of stoichiometric Pt_3Sn alloy particles, with an average size of ∼3–4 nm.

(5) All of the metallic particles in the 900N and E270 catalysts have an equiaxed shape. A significant number of metallic particles in the 500N sample have an elongated shape, probably reflecting the partially reacted character of this material and incomplete reaction between Pt and SnO_2 particles in physical contact.

(6) In both 500N and 900N, large amounts of unreacted SnO_2 remain, which could have an effect on the behavior of electrodes prepared from these catalysts.

Acknowledgment

We thank Dr. David Thompsett from the Johnson Matthey Technology Center and Dr. Emory DeCastro from De-Nora (E-TEK Division, Somerset, NJ) for supplying the Pt–Sn catalyst samples. This research was supported by the Office of Advanced Automotive Technology (OAAT) of the U.S. Department of Energy under contract no. DE-AC0376SF00098.

References

[1] R. Srinivasan, R.J. De Angeles, B.H. Davis, J. Catal. 106 (1987) 449.
[2] R. Srinivasan, R.J. De Angeles, B.H. Davis, J. Catal. Lett. 4 (1990) 303.
[3] R. Srinivasan, L.A. Rice, B.H. Davis, J. Catal. 129 (1991) 257.
[4] R. Srinivasan, B.H. Davis, Appl. Catal. 87 (1992) 45.
[5] R. Srinivasan, B.H. Davis, Plat. Metals Rev. 36 (1992) 151.
[6] R. Srinivasan, R. Sharma, S. Su, B.H. Davis, Catal. Today 21 (1994) 83.
[7] V.I. Kuznetsov, A.S. Belyi, E.N. Yurchenko, M.D. Smolikov, M.T. Protasova, E.V. Zatolokina, V.K. Duplayakin, J. Catal. 99 (1986) 159.
[8] J. Schwank, K. Balakrishnamand A. Sachdev, in: L. Guczi, F. Solymosi, P. Tetenyi (Eds.), Proc. 10th Int. Congr. Catalysis, Part A (1993) p. 905.
[9] H.A. Gasteiger, N.M. Markovic, P.N. Ross, J. Phys. Chem. 99 (1995) 8945.

[10] H.A. Gasteiger, N.M. Markovic, P.N. Ross, Catal. Lett. 36 (1996) 1.
[11] T.J. Schmidt, H.A. Gasteiger, R.J. Behm, J. New Mat. Electrochem. Systems 2 (1999) 27.
[12] M. Goetz, H. Wendt, Electrochim. Acta 43 (1998) 3637.
[13] E.M. Crabb, R. Marshall, D. Thompsett, J. Electrochem. Soc. 147 (2000) 4440.
[14] V. Radmilovic, H.A. Gasteiger, P.N. Ross Jr., J. Catal. 154 (1995) 98.
[15] A.K. Datye, D.J. Smith, Catal. Rev.-Sci. Eng. 34 (1992) 129.
[16] M.J. Yacaman, M. Avalos-Borja, Catal. Rev.-Sci. Eng. 34 (1992) 55.
[17] H. Poppa, Catal. Rev.-Sci. Eng. 35 (1993) 359.
[18] M.L. Sattler, P.N. Ross, Ultramicroscopy 20 (1986) 21.
[19] D.J. Smith, L.D. Marks, Ultramicroscopy 16 (1985) 101.
[20] M.J. Yacaman, J.M. Dominguez, J. Catal. 64 (1980) 213.
[21] See http://ncem.lbl.gov/frames/microscopes&facilities.htm for a description of NCEM microscopes.
[22] G. del Angel, S. Alerasool, J.M. Domingues, R.D. Gonzales, R. Gomez, Surf. Sci. 224 (1989) 407.
[23] V. Radmilovic, H.A. Gasteiger, P.N. Ross Jr., in: Proc. MSA, 1994, p. 782.
[24] J.-O. Malm, M.A. O'Keefe, in: Proc. EMSA, 1993, p. 974.
[25] T. Chojnacki, K.R. Krause, L.D. Schmidt, J. Catal. 128 (1991) 161.
[26] V. Radmilovic, M. O'Keefe, R. Kilaas, EUREM'96, Dublin, 1996, CD-ROM, file: M/M2/Radmilov.
[27] C.G. Granquist, R.A. Buhrman, J. Catal. 42 (1976) 477; P.J. Harris, E.D. Boyes, J.A. Cairns, J. Catal. 82 (1983) 17.
[28] W.J. de Ruijter, R. Sharma, M.R. McCartney, D.J. Smith, Ultramicroscopy 57 (1995) 409.
[29] S. Iijima, T. Ichihashi, Phys. Rev. Lett. 56 (1986) 616.
[30] P.M. Ajayan, L.D. Marks, Phys. Rev. Lett. 63 (1989) 279.
[31] G. Fuchs, D. Neiman, H. Poppa, Langmuir 7 (1991) 2853.
[32] M.-H. Yao, D.J. Smith, A.K. Datye, Ultramicroscopy 52 (1993) 282.
[33] U. Dahmen, MRS Bull. 24 (1994) 341.
[34] J. Dundurs, L.D. Marks, P.M. Ajayan, Philos. Mag. A 57 (1988) 605.
[35] M. Hansen, Constitution of Binary Alloys, McGraw-Hill, New York, 1958, pp. 1141-1142.
[36] I.R. Harris, M. Norman, A.W. Brayant, J. Less-Common Met. 16 (1968) 427.
[37] TAPP V. 2.0 is published by: ES Microware, Inc., 2234 Wade Court, Hamilton.